RESEARCH ARTICLE

PI3K Signaling Through the Dual GTPase–Activating Protein ARAP3 Is Essential for Developmental Angiogenesis

Laure Gambardella,[1] Myriam Hemberger,[2,3] Bethany Hughes,[1] Enrique Zudaire,[4] Simon Andrews,[5] Sonja Vermeren[1*†]

One function of phosphoinositide 3-kinase α (PI3Kα), which generates the lipid second messenger phosphatidylinositol 3,4,5-trisphosphate [PtdIns(3,4,5)P$_3$], is its regulation of angiogenesis in the developing embryo and in pathological situations. ARAP3 is a PtdIns(3,4,5)P$_3$- and Rap-activated guanosine triphosphatase (GTPase)–activating protein (GAP) for the small GTPases RhoA and Arf6. Here, we show that deleting *Arap3* in the mouse caused embryonic death in mid-gestation due to an endothelial cell–autonomous defect in sprouting angiogenesis. Explants taken at a developmental stage at which no defect was yet present reproduced this phenotype ex vivo, demonstrating that the defect was not secondary to hypoxia, placental defects, or organ failure. In addition, knock-in mice expressing an ARAP3 point mutant that cannot be activated by PtdIns(3,4,5)P$_3$ had angiogenesis defects similar to those of *Arap3*$^{-/-}$ embryos. Our work delineates a previously unknown signaling pathway that controls angiogenesis immediately downstream of PI3Kα through ARAP3 to the Rho and Arf family of small GTPases.

INTRODUCTION

The generation of a circulatory system during embryonic development involves the formation of a primitive vascular plexus (vasculogenesis) that is later remodeled by angiogenesis into an organized, treelike structure comprising arteries and veins, which are connected by a network of capillaries. This remodeling occurs by three distinct mechanisms: (i) sprouting of new vessels, (ii) intussusception (splitting of existing vessels), and (iii) pruning (*1*, *2*). In the adult, angiogenesis reappears in pathological situations such as arteriosclerosis, tumor growth, or wound healing. The major regulator of angiogenesis is hypoxia, which induces the local production of vascular growth factors such as vascular endothelial growth factor (VEGF). This in turn induces signaling downstream of VEGF receptors in endothelial cells. Complex signaling processes, many components of which remain poorly understood, regulate in concert the tight coordination among cell proliferation, differentiation, and migration required for the generation of a healthy vascular system.

Agonist-activated (class I) phosphoinositide 3-kinases (PI3Ks) generate the lipid second messengers phosphatidylinositol 3,4,5-trisphosphate [PtdIns(3,4,5)P$_3$] and phosphatidylinositol 3,4-bisphosphate [PtdIns(3,4)P$_2$], which localize to the inner leaflet of the plasma membrane. Class I PI3Ks are essential regulators of a large number of important physiological processes. Four different heterodimeric class I PI3Ks exist, which couple to either growth factor receptor tyrosine kinases (class IA, comprising a p110α, -β, or -δ catalytic subunit and a p85 or p55 type adaptor protein) or heterotrimeric guanosine 5′-triphosphate (GTP)–binding protein (G protein)–coupled receptors (class IB, with a p110γ catalytic subunit and a p101 or p84 regulatory subunit) (*3*). PI3K mouse models have indicated that class IA PI3Ks, in particular those containing p110α (PI3Kα), regulate angiogenesis both during embryonic development and in pathological situations. Loss of p110α, or of its catalytic activity, or of the class IA PI3K regulatory subunits (which leads to the degradation of p110 subunits) causes embryonic lethality at mid-gestation as a result of an angiogenesis defect (*4*, *5*). About 50 PI3K effectors have been identified, many of which contain pleckstrin homology (PH) domains, which specifically bind to PtdIns(3,4,5)P$_3$. PI3K effectors are regulated by PtdIns(3,4,5)P$_3$ by translocation to the plasma membrane or the induction of a conformational change. Many PtdIns(3,4,5)P$_3$-binding proteins are regulators of small guanosine triphosphatases (GTPases) of the Rho and Arf families.

ARAP3 is one such PI3K effector, which we identified as part of a targeted proteomic screen for PtdIns(3,4,5)P$_3$-binding proteins (*6*). ARAP3 is a dual GTPase–activating protein (GAP) for RhoA and Arf6. It is regulated by PtdIns(3,4,5)P$_3$ both catalytically—its Arf GAP activity is PtdIns(3,4,5)P$_3$ dependent—and by recruitment to the plasma membrane in a PH domain–dependent manner (*7*). The most N-terminal PH domain of ARAP3 mediates its interaction with PtdIns(3,4,5)P$_3$ (*7*, *8*).

Here, we show that deleting ARAP3 in the mouse leads to a sprouting angiogenesis defect, which resembles that described in knock-in mice carrying a catalytically dead p110α (D933A) allele. Furthermore, we demonstrate that introducing point mutations in conserved arginine residues in ARAP3's most N-terminal PH domain (R302,303A), thus interfering with the regulatory input of PI3K into ARAP3, phenocopies the angiogenesis defect of *Arap3*$^{-/-}$ mice. Thus, signaling through ARAP3 immediately downstream of PI3K is required for developmental angiogenesis.

RESULTS

Arap3$^{-/-}$ mice die as a result of an endothelial cell–dependent defect in mid-gestation

We generated a conditional *Arap3* knockout mouse (*Arap3*$^{fl/fl}$) to elucidate ARAP3's physiological function (fig. S1). Crossing the *Arap3*$^{fl/fl}$ mouse

[1]Inositide Laboratory, The Babraham Institute, Cambridge CB22 3AT, UK. [2]Epigenetics and Development Laboratory, The Babraham Institute, Cambridge CB22 3AT, UK. [3]Centre for Trophoblast Research, University of Cambridge, Downing Street, Cambridge CB2 3EG, UK. [4]Angiogenesis Core Facility, National Cancer Institute, National Institutes of Health, Gaithersburg, MD 20892–465, USA. [5]Bioinformatics, The Babraham Institute, Cambridge CB22 3AT, UK.
*Née Krugmann.
†To whom correspondence should be addressed. E-mail: sonja.vermeren@bbsrc.ac.uk

with a germline *Cre* deletor (*9*) to generate *Arap3*⁻/⁻ mice resulted in embryonic death around E11 (embryonic day 11) (table S1). At E10.5, *Arap3*⁻/⁻ embryos were pale, small in size, and had various developmental defects, including a characteristically wrinkled yolk sac (fig. S2). All mutant embryos displayed regular heartbeats, causing visible blood flow in the large vessels (fig. S3). In *Arap3*⁻/⁻ embryos, ARAP3 protein was not present, whereas the abundance of other ARAP family members ARAP1 and ARAP2 was not affected (Fig. 1, A and B). Because growth arrest followed by deterioration until death at mid-gestation could indicate a placental defect, we compared placentas of *Arap3*⁻/⁻ embryos with those from *Arap3*⁺/⁻ embryos and wild-type controls and found a defect in labyrinth formation in placentas from *Arap3*⁻/⁻ (but not from *Arap3*⁺/⁻) embryos; however, spongiotrophoblast and giant cell layers were not affected (fig. S4). Labyrinth development depends on the proper differentiation and fusion of the trophoblast into highly specialized syncytiotrophoblast cells, as well as on the invasion of allantoic mesoderm to form the labyrinthine vasculature. To determine in which of these two cell populations the defect of *Arap3*⁻/⁻ placentas resides, we deleted *Arap3* in the embryo proper and in the extra-embryonic mesoderm, but not in the trophoblast, with *Sox2Cre* (*10*). *Arap3*ᶠˡ/⁻ *Sox2Cre*⁺ embryos displayed defects identical to those of *Arap3*⁻/⁻ embryos (fig. S2), indicating that the observed phenotype was due to a defect in the labyrinthine vasculature and not intrinsic to the trophoblast compartment. This suggested that lack of ARAP3 affected vascular development. Accordingly, in situ hybridizations revealed the presence of *Arap3* in blood vessels in both the yolk sac and the embryo (fig. S5A). We used *Tie2Cre* to specifically delete *Arap3* in the endothelial compartment (*11*) and confirmed that endothelial cell populations derived from *Arap3*⁻/ᶠˡ *Tie2Cre*⁺ embryos lacked ARAP3 protein (Fig. 1C). This resulted in embryonic lethality and a phenotype identical to that of *Arap3*⁻/⁻ embryos (fig. S2), indicating *Arap3*⁻/⁻ embryos died as a result of an endothelial cell–autonomous defect.

Vasculature of *Arap3*⁻/⁻ yolk sacs and embryos is disorganized

To characterize the nature of this endothelial defect, we stained yolk sacs from *Arap3*⁻/⁻ and wild-type mice for endomucin, a marker for mature endothelial cells. Remodeling of the primary vascular plexus into large vessels and a connecting capillary network did not occur in the *Arap3*⁻/⁻ and *Arap3*⁻/ᶠˡ *Tie2Cre*⁺ yolk sacs (figs. S5B and S6A). Instead, they exhibited areas with unevenly sized vessel lumens, some of which were large, giving an impression of accumulations of endothelial cells (arrows) in whole-mount–stained samples. Sections of yolk sac from *Arap3*⁻/⁻ mice revealed large open spaces, which were lined by endothelial cells (fig. S6B). This abnormally loose association of mesodermal and endodermal layers in *Arap3*⁻/⁻ yolk sacs is likely to be responsible for their distinctive wrinkled appearance. Given that in the sections the spaces appeared devoid of embryonic blood cells, that *Arap3*⁻/⁻ embryos and yolk sacs were pale (with the exception of a few blood patches in the yolk sacs), and that the hemangioblast is thought to be a common precursor for endothelial and hematopoietic structures, we assessed whether hematopoiesis was affected in *Arap3*⁻/⁻ yolk sacs. We performed methylcellulose colony assays from yolk sac suspensions and obtained similar numbers of erythroid and myeloid colonies from control and *Arap3*⁻/⁻ samples, thereby excluding a hematopoiesis defect (fig. S6C). In addition, analysis of freshly isolated yolk sac suspensions by fluorescence-activated cell sorting (FACS) indicated a similar percentage of embryonic red blood cells in *Arap3*⁻/⁻ and control yolk sacs (fig. S6D), suggesting that blood cells may accumulate in a small number of places in the loosely assembled *Arap3*⁻/⁻ yolk sacs and be prone to getting lost during subsequent dissections, fixation, and staining steps.

When analyzing endomucin-stained *Arap3*⁻/⁻ embryos, we found that remodeling of the primary plexus had not progressed in an orderly fashion

compared to wild-type controls (Fig. 1D). Although heterozygous *Arap3*⁺/⁻ animals showed slightly delayed vascularization at E10.5 (Fig. 1E), this was no longer apparent at E11.5 (fig. S7). In contrast, *Arap3*⁻/⁻ and *Arap3*ᶠˡ/⁻ *Tie2Cre*⁺ embryos were defective in vascular maturation and remodeling (Fig. 1, F and G). This was most apparent in embryonic midbrains, where the capillary network, when viewed as a whole, was replaced by a large accumulation of endothelial cells, reminiscent of the structures observed in the mutant yolk sacs (Fig. 2, A to D). Analysis of confocal sections through the embryonic heads indicated that these structures corresponded to endothelial cell–lined sinuses, which replaced the capillary network in wild-type and *Arap3*⁻/⁺ midbrains (Fig. 2, E to H). To address whether the underlying rea-
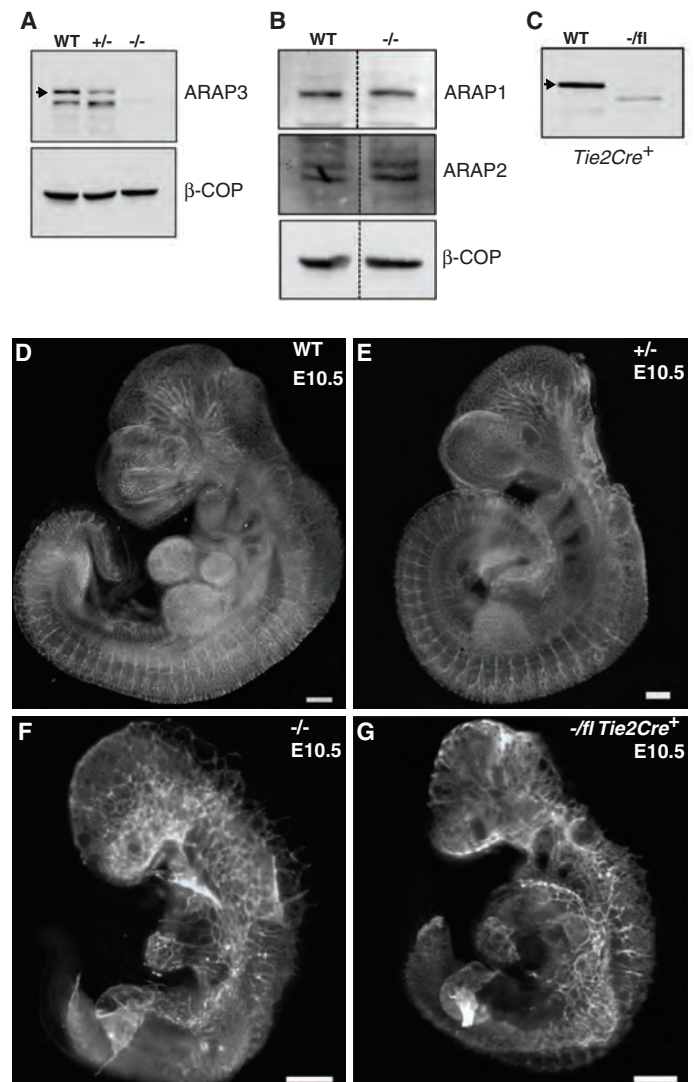

Fig. 1. Vascular remodeling is affected in *Arap3*⁻/⁻ embryos. (**A** to **C**) Lysates from entire E10.5 embryos (A and B) or E9.5 yolk sac–derived endothelial cell populations (C) were subjected to SDS-PAGE and Western blotting with antisera specific for ARAP3 (A and C), ARAP1 and ARAP2 (B), or the loading control β-COP. (**D** to **G**) Wild-type (WT) (n = 24), *Arap3*⁺/⁻ (+/−) (n = 12), *Arap3*⁻/⁻ (−/−) (n = 18), and *Arap3*ᶠˡ/⁻ *Tie2Cre*⁺ E10.5 (−/fl Tie2Cre⁺) (n = 7) embryos were whole-mount–stained for endomucin. Representative images are shown. Scale bars, 0.25 mm.

son for formation of this structure might be uncontrolled endothelial cell growth, we analyzed immunostaining for phosphohistone H3, a marker of proliferation, and found that the rate of endothelial cell division was not increased in $Arap3^{-/-}$ midbrains (fig. S8). Similarly, when we examined staining of phosphohistone H3 in wild-type and $Arap3^{-/-}$ yolk sacs, we found no increased proliferation in the absence of ARAP3 (fig. S8), indicating that this phenotype was not caused by general overproliferation of the endothelial compartment but was due to a defect in angiogenic remodeling in $Arap3^{-/-}$ animals.

ARAP3 is required for angiogenesis rather than vasculogenesis

To address whether the defects in $Arap3^{-/-}$ embryos and yolk sacs could be secondary effects due to hypoxia, organ failure, or placental insufficiency, we cultured the para-aortic splanchnopleural (P-Sp) regions of E8.5 control and $Arap3^{-/-}$ embryos (before the onset of any defects in $Arap3^{-/-}$ embryos) on stromal feeder cells. This system recapitulates the different steps of blood vessel development and hematopoiesis ex vivo, with explants initially forming a vascular bed by vasculogenesis and then developing a vascular network by angiogenesis (12). $Arap3^{-/-}$ vascular networks that were generated by angiogenesis were less complex than in controls, containing fewer but thicker branches, rather than the well-interconnected thin branches of control networks (Fig. 3, A and B). $Arap3^{-/-}$ P-Sp explants also contained characteristic endothelial cell accumulations, which, when viewed by phase-contrast microscopy, were reminiscent of the large endothelial sinuses replac-

ing capillary networks seen in $Arap3^{-/-}$ yolk sacs and embryonic midbrains (Fig. 3B, stars). In summary, P-Sp explants confirmed that loss of $Arap3$ conferred a defect in angiogenesis, rather than vasculogenesis, and showed that this defect was not secondary to hypoxia, placental insufficiency, or organ failure.

ARAP3 regulates sprouting angiogenesis

To evaluate the effects of $Arap3$ deficiency on angiogenesis ex vivo, we performed allantois explants, in which the allantois of the E8.5 embryo is cultured on fibronectin-coated tissue culture plastic and within hours produces a tubular endothelial network by sprouting angiogenesis (13, 14). Although we could not detect differences between allantoises from E8.5 wild-type and $Arap3^{-/-}$ embryos (fig. S9), the networks generated from $Arap3^{-/-}$ allantoises were less complex and smaller than those from controls (Fig. 3, C and D). We used computer algorithms to "skeletonize" the allantois explants (Fig. 3E) and to count the number of branching points and correct for the overall size of the analyzed explants to derive each explant's "branching index," which counts the numbers of junctions per square millimeter. We plotted branching indices and statistically analyzed any differences obtained (Fig. 3F). Average $Arap3^{-/-}$ branching indices were significantly smaller than those of controls, indicating that loss of ARAP3 caused a decreased ability of the explants to perform sprouting angiogenesis in the context of allantois explants.

To ascertain whether this conclusion held true in vivo, we analyzed the embryonic hindbrain (Fig. 4, A to D), where new vessels sprout in a tem-
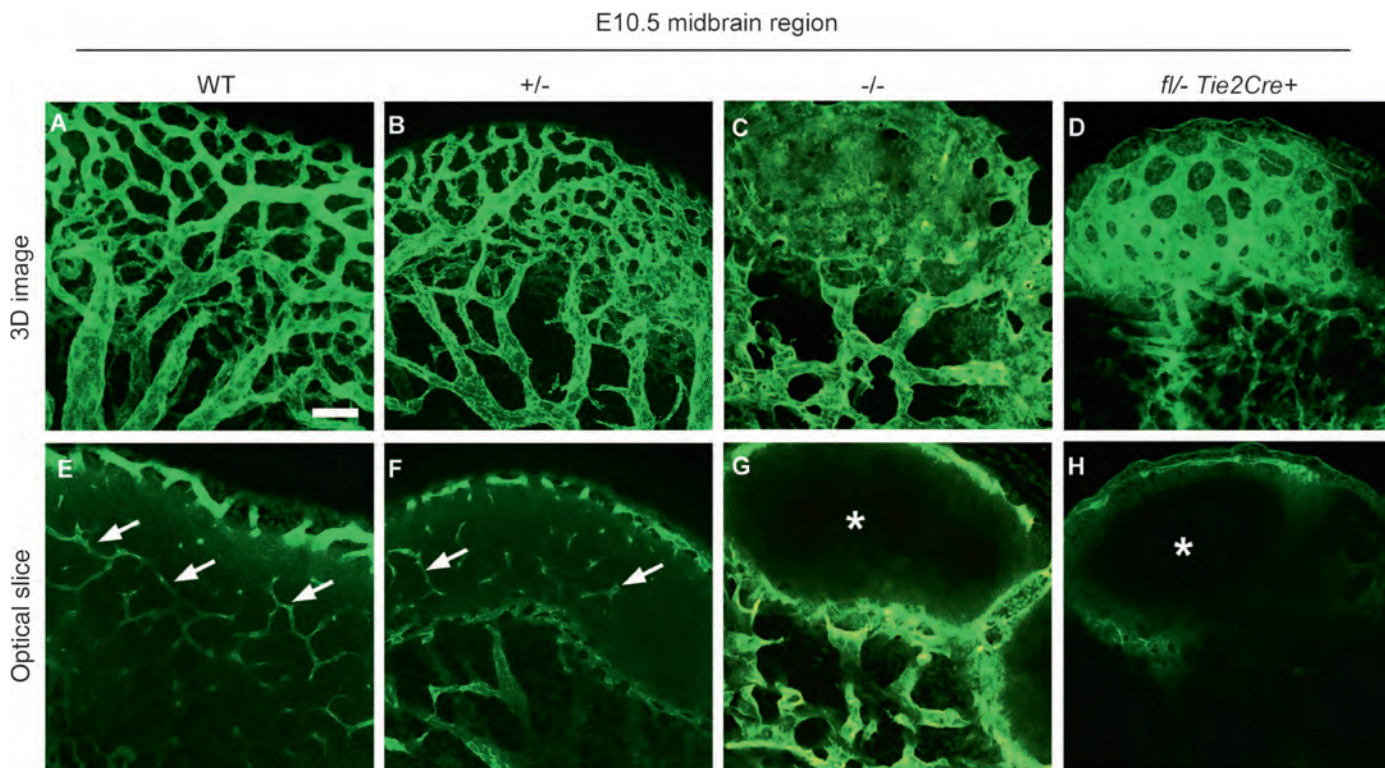

Fig. 2. $Arap3^{-/-}$ embryonic midbrains display disordered capillary networks. (A to D) Representative 3D reconstructions of endomucin whole-mount–stained E10.5 midbrains from WT (n = 14), $Arap3^{+/-}$ (+/–) (n = 8), $Arap3^{-/-}$ (–/–) (n = 11), and $Arap3^{-/fl}$ Tie2Cre$^+$ (–/fl Tie2Cre$^+$) (n = 4) embryos. Scale bar, 90 μm. Capillary networks are apparent in midbrains of WT and $Arap3^{+/-}$ embryos, but not in those of $Arap3^{-/-}$ and $Arap3^{-/fl}$ Tie2Cre$^+$ embryos. (E to H) Optical slices of the midbrains shown in (A) to (D). Capillaries in WT and $Arap3^{+/-}$ midbrains are indicated by arrows. $Arap3^{-/-}$ and $Arap3^{-/fl}$ Tie2Cre$^+$ heads are characterized by large open sinuses, indicated by asterisks (*).

porally and spatially well-defined manner from the perineural plexus into the neural tube to branch out, forming the subventricular plexus (*15*). As expected, we saw capillary sprouting and extensive branching in E10.5 wild-type hindbrains (Fig. 4A). In contrast, no capillary sprouting from the perineural plexus toward the midline was observed in hindbrains from

$Arap3^{-/-}$ embryos (Fig. 4C). We noted that the complexity of the network formed was reduced in E10.5 hindbrains from $Arap3^{+/-}$ embryos, which had shorter vessels, incompletely formed interconnections between parallel running vessels, and significantly fewer branching points (Fig. 4, B and D). As with the other delays in angiogenesis that were observed in $Arap3^{+/-}$ embryos, these differences between wild-type and $Arap3^{+/-}$ hindbrains were no longer apparent at E11.5 (fig. S10A). In keeping with our observation of mild angiogenesis defects in $Arap3^{+/-}$ embryos, and only discernible at early developmental time points, our analysis of retinal sprouting angiogenesis, the best-characterized system for the analysis of angiogenesis (*16*), did not
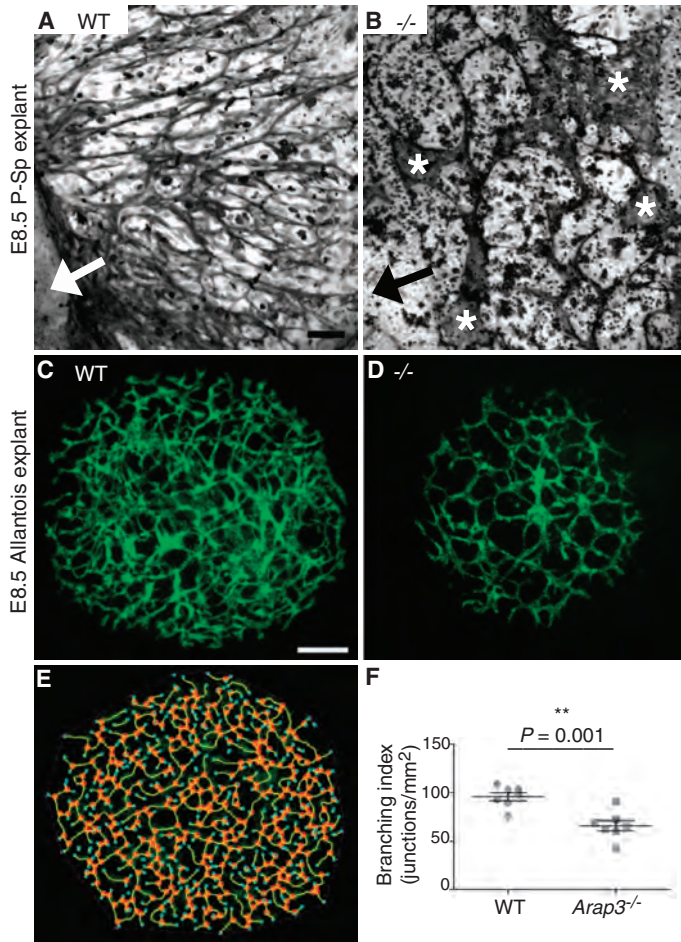

Fig. 3. Loss of ARAP3 confers a defect in sprouting angiogenesis ex vivo. (**A** and **B**) P-Sp regions taken from E8.5 WT and $Arap3^{-/-}$ embryos (−/−) were grown on OP9 feeder cells for 2 weeks. Endothelial cells were labeled with antibodies against endomucin and CD31. Representative images from 17 WT and 4 $Arap3^{-/-}$ explants are shown. Arrows indicate the position of the vascular beds, and asterisks indicate accumulation of endothelial cells in the $Arap3^{-/-}$ explant. Scale bar, 160 μm. (**C** and **D**) Representative images of allantois explants taken from WT (*n* = 25) and $Arap3^{-/-}$ (*n* = 10) embryos. Explants were grown on fibronectin-coated plastic dishes for 18 hours, fixed, and labeled with antibodies against endomucin and VE-cadherin. Scale bar, 0.2 mm. (**E**) Example of a skeletonized WT allantois explant. For analysis, all allantois explants were skeletonized, where branches were marked (shown in yellow) and branching points (large red circles) and branch end points (small blue circles) were established by computer algorithms. Numbers of branching points counted were corrected for the sizes of the individual explants to allow a fair comparison. A branching index was thus obtained for each analyzed explant. (**F**) Amalgamated branching indices. Error bars indicate SEM. Statistical significance was determined with Student's *t* test.
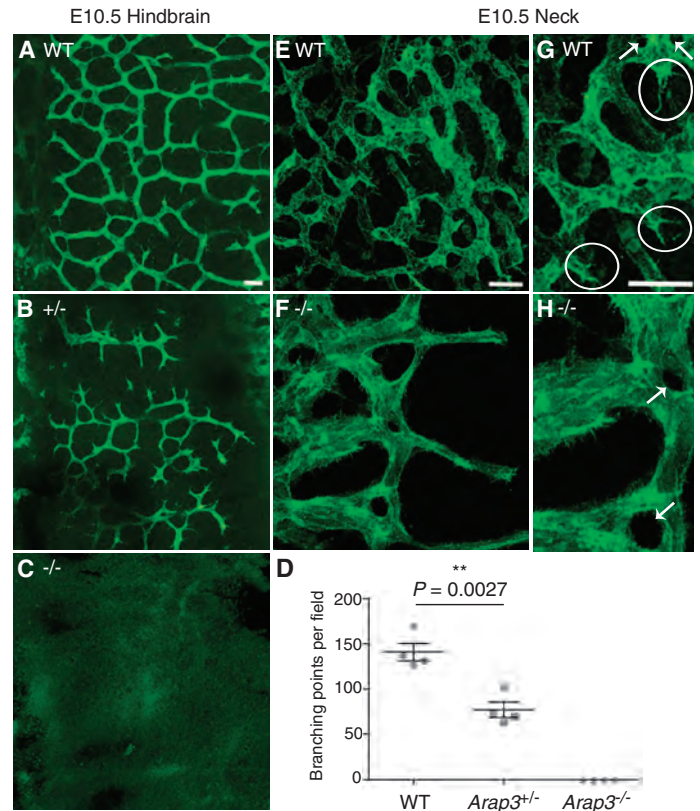

Fig. 4. ARAP3 is required for sprouting angiogenesis in vivo. (**A** to **C**) Hindbrains (E10.5) from WT, $Arap3^{+/-}$ (+/−), and $Arap3^{-/-}$ (−/−) were dissected, and the microvascular network was visualized by labeling endomucin. Representative confocal images taken from the ventricular side are shown; the midline is to the left of the images. Sprouting between parallel running vessels is delayed in $Arap3^{+/-}$ hindbrains at this age, whereas sprouting angiogenesis is absent in $Arap3^{-/-}$ hindbrains. (**D**) Amalgamated numbers of branching points in WT, $Arap3^{+/-}$, and $Arap3^{-/-}$ hindbrains. Each point in the graph represents the average from three individual fields of view (0.4 mm^2) taken from each of four hindbrains analyzed per genotype. Statistical significance between WT and $Arap3^{+/-}$ hindbrains was determined by Student's *t* test. The $Arap3^{-/-}$ hindbrains were excluded from the statistical analysis because they were not quantifiable. (**E** and **F**) E10.5 necks were analyzed by confocal microscopy. Each photo shows a 3D reconstruction; note the reduced complexity and increased vessel diameter in $Arap3^{-/-}$ necks. (**G** and **H**) Enlarged sections from the images shown in (E) and (F) illustrate both sprouting angiogenesis (ovals) and intussusception (arrows) taking place in WT necks, whereas in $Arap3^{-/-}$ tissue, only sites of intussusception are apparent (arrows). Scale bars, 40 μm.

indicate any significant defects in $Arap3^{+/-}$ retinas. No differences were found in terms of either radial expansion or the complexity of the network formed as assessed by the branching index (fig. S10B). However, we were able to analyze the nature of the defect in $Arap3^{-/-}$ animals by studying the embryonic region below the otic vesicle but above the first somite (we refer to this region as the embryonic "neck") (Fig. 4, E and F). We observed abundant new sprouts in wild-type tissue, led by characteristic filopodia-carrying tip cells (Fig. 4G, ovals) and sites of intussusception (Fig. 4G, arrows). In contrast, $Arap3^{-/-}$ necks contained no new sprouts, although there were sites of intussusception (Fig. 4, F and H). Moreover, $Arap3^{-/-}$ necks contained fewer but thicker vessels. The enlarged vessel diameter in $Arap3^{-/-}$ embryonic necks might represent a hypoxia-driven attempt by the embryo to increase oxygen supply as a compensatory mechanism in the absence of the ability of the existing vessels to form new branches.
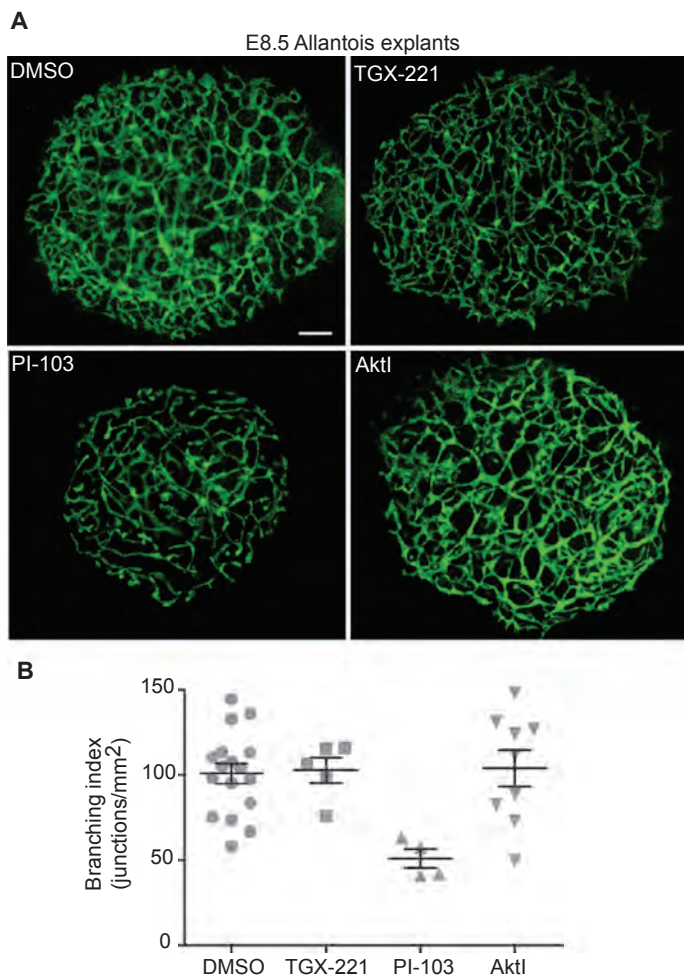
A

B

Fig. 5. PI3K signaling is required for sprouting angiogenesis. (A) Allantois explants were taken from WT embryos and treated with DMSO, 40 nm TGX-221, 0.25 μM PI-103, or 0.3 μM AktI and grown on fibronectin-coated plastic for 18 hours. Explants were fixed and labeled with antibodies against endomucin and VE-cadherin, and representative images were taken. Scale bar, 0.2 mm. (B) Amalgamated branching indices from all explants analyzed in this context. Error bars indicate SEM. PI-103 treatment is the only condition that induces a significant difference ($P < 0.001$) as evaluated by univariate analysis of variance with Games-Howell post hoc test.

Together, our in vivo analyses suggested that in the embryo proper, ARAP3 is important for sprouting angiogenesis during early embryonic development, whereas it is dispensable for intussusceptive growth.

PI3Kα regulates sprouting angiogenesis

Although a role of ARAP3 in angiogenesis was not previously known, a prominent function of PI3Kα in developmental angiogenesis has been reported (5). Endothelial cell–specific loss of the catalytic p110α subunit or knocking in of a point mutation (D933A) that renders p110α catalytically dead caused embryonic lethality at mid-gestation with a phenotype similar to the one we present here for $Arap3^{-/-}$ embryos. Because the role of PI3K in sprouting angiogenesis in allantois assays had not yet been addressed, we treated explants with PI-103, which inhibits p110α with the highest efficiency (17), or with TGX-221, a compound specific for the p110β catalytic subunit (18). Although TGX-221 did not affect sprouting in allantois explants, PI-103 caused a significant reduction in sprouting and complexity (Fig. 5) to a comparable extent as in $Arap3^{-/-}$ explants. This agrees with published data that PI3Kα, but not PI3Kβ, is essential for developmental angiogenesis (5).

The serine-threonine kinase Akt [also known as protein kinase B (PKB)] is the best-characterized class I PI3K effector. Akt regulates multiple pathways that affect cell metabolism, growth, proliferation, and apoptosis. Three Akt isoforms exist (Akt1, Akt2, and Akt3), of which Akt1 has been implicated in angiogenesis. Although either loss or overexpression of $Akt1$ interferes with the formation of mature, healthy vessels in pathological angiogenesis (19, 20), the role of Akt in developmental angiogenesis is less clear-cut. $Akt1^{-/-}$ mice are viable but have placental defects (21), whereas some double and triple knockouts cause embryonic lethality because of various severe defects (22). We treated allantois explants with Akt inhibitor VIII (AktI), a selective, noncompetitive inhibitor of Akt1 and Akt2 (23), to analyze the role of Akt in developmental angiogenesis ex vivo. Sprouting and branching indices were not affected in AktI-treated allantois explants (Fig. 5), indicating that Akt activity is not essential for angiogenesis in this context.

ARAP3 lies immediately downstream of PI3K in the regulation of angiogenesis

The regulation of ARAP3 by PtdIns(3,4,5)P$_3$ is twofold. ARAP3 is recruited to the plasma membrane in a PI3K-dependent manner, which brings it into proximity of its substrates RhoA-GTP and Arf6-GTP. In addition, ARAP3's Arf GAP activity requires PtdIns(3,4,5)P$_3$ (6). We found that the interaction between ARAP3 and PtdIns(3,4,5)P$_3$ was PH domain–mediated (8). In the context of full-length ARAP3, mutagenesis of two conserved arginine residues within the predicted variable loop between the β1 and the β2 strands of the most N-terminal PH domain abrogated binding to PtdIns(3,4,5)P$_3$ and interfered with PI3K-dependent plasma membrane translocation of full-length ARAP3 (6, 8). To address the role of PI3K as a regulator of ARAP3 in angiogenesis in vivo, we generated a knock-in mouse model (fig. S11), which contained the R302,303A double point mutation in ARAP3's most N-terminal PH domain to interrupt binding to PtdIns(3,4,5)P$_3$ and therefore uncouple ARAP3 from activation through PI3K.

Similar to $Arap3^{-/-}$ mice, $Arap3^{R302,303A/R302,303A}$ knock-in mice were embryonically lethal at E11 (table S2), with homozygous mutants phenocopying $Arap3^{-/-}$ embryos, although the presence of the point mutation did not interfere with the abundance of ARAP3 protein (Fig. 6A). $Arap3^{-/-}$ and $Arap3^{R302,303A/R302,303A}$ embryos were grossly morphologically similar (Fig. 6, B and C) and had wrinkled yolk sacs (fig. S12, A and B). Similar to $Arap3^{-/-}$ embryos, the midbrains of $Arap3^{R302,303A/R302,303A}$ embryos were characterized by an endothelial cell–lined sinus (Fig. 6, D to G). However, in E10.5 $Arap3^{R302,303A/R302,303A}$ hindbrains, we observed no sprouting toward the midline, as had been the case in $Arap3^{-/-}$ embryos (fig. S12,

C and D). Similarly, $Arap3^{R302,303A/R302,303A}$ embryonic necks displayed less abundant vessels with larger diameters and were devoid of sprouting angiogenesis (Fig. 6, H and I), as described for $Arap3^{-/-}$. Similarities between the null and knock-in mice were also apparent ex vivo, because $Arap3^{R302,303A/R302,303A}$ P-Sp explants displayed patches of accumulated endothelial cells (fig. S12, E and F), and $Arap3^{R302,303A/R302,303A}$ allantois explants were characterized by reduced complexity, less sprouting, and smaller branching indices than controls (fig. S12, G to I). This showed that interfering with PI3K-dependent regulation of ARAP3 caused the same defects in angiogenic remodeling as did complete ablation of ARAP3. Thus, ARAP3 lies immediately downstream of PI3K in the regulation of embryonic angiogenesis.

ARAP3 signals through modulating the catalytic activities of RhoA and Arf6

We previously showed that ARAP3 is a PtdIns(3,4,5)P$_3$-dependent Arf6 GAP and a PI3K- and Rap-regulated RhoA GAP. We also demonstrated that introducing a point mutation in the most N-terminal PH domain of ARAP3 interferes with its binding to PtdIns(3,4,5)P$_3$ and renders the protein catalytically inactive as an Arf GAP in vitro, although in vitro basal Rho GAP activity was unaffected. In the context of cell-based assays, this point mutant behaves as a catalytically dead mutant, most likely because it is no longer recruited to the plasma membrane where its substrate is located (6, 7). We were unable to address whether the activities of RhoA and Arf6 were altered in endothelial cells derived from $Arap3^{-/-}$ and $Arap3^{R302,303A/R302,303A}$ embryos compared to those derived from wild-type embryos because we were unable to culture embryonic cells to generate sufficient numbers of cells required for such assays. As a compromise, we used RNA interference (RNAi)–mediated knockdown of ARAP3. Knocking down ARAP3 with a pool of four specific RNAi oligos was not efficient in primary human umbilical vein endothelial cells (HUVECs) (fig. S13), but we obtained reproducible efficient knockdown of ARAP3 (>85%) in the immortalized HUVEC line EA926.hy (Fig. 7, A and B), which has been extensively characterized and preserves endothelial characteristics over many passages in culture (24). When analyzing the average activity of Arf6 in the transfected cells, we noticed that VEGF stimulation weakly activated Arf6-GTP in control transfected cells, but not in ARAP3 RNAi-transfected cells (Fig. 7, C and D). Similar to p110α^{D933A} knock-in cells (5), the global amount of RhoA-GTP was reduced in ARAP3-depleted cells growing in the presence of fetal bovine serum (Fig. 7E). In addition, we analyzed RhoA activity after stimulation with VEGF, which is reported to activate RhoA (25), as well as PI3K and therefore ARAP3. Serum-starved cells transfected with ARAP3 RNAi had a greater response to VEGF than control cells (Fig. 7F). In summary, we observed subtle changes in global Arf6 and RhoA activities in immortalized HUVECs in which ARAP3 was knocked down. This suggests that ARAP3-dependent regulation of angiogenesis may occur by signaling through its effectors Arf6 and RhoA.

DISCUSSION

Here, we demonstrate with genetic mouse models that a crucial physiological function of ARAP3 lies in the regulation of developmental sprouting angiogenesis. In addition, using a PH domain point mutation knock-in mouse, in which ARAP3 is uncoupled from activation through PtdIns(3,4,5)P$_3$, we show that the regulatory input of PI3K into ARAP3 is required for its function in angiogenesis. This work identifies ARAP3 as a key effector of PI3K in the regulation of angiogenesis and demonstrates that the observed phenotype is not due to the loss of a multidomain protein, which may serve as a scaffold.

A previously demonstrated role of p110α lies in the control of cell metabolism, proliferation, or survival through signaling to Akt (17, 26).
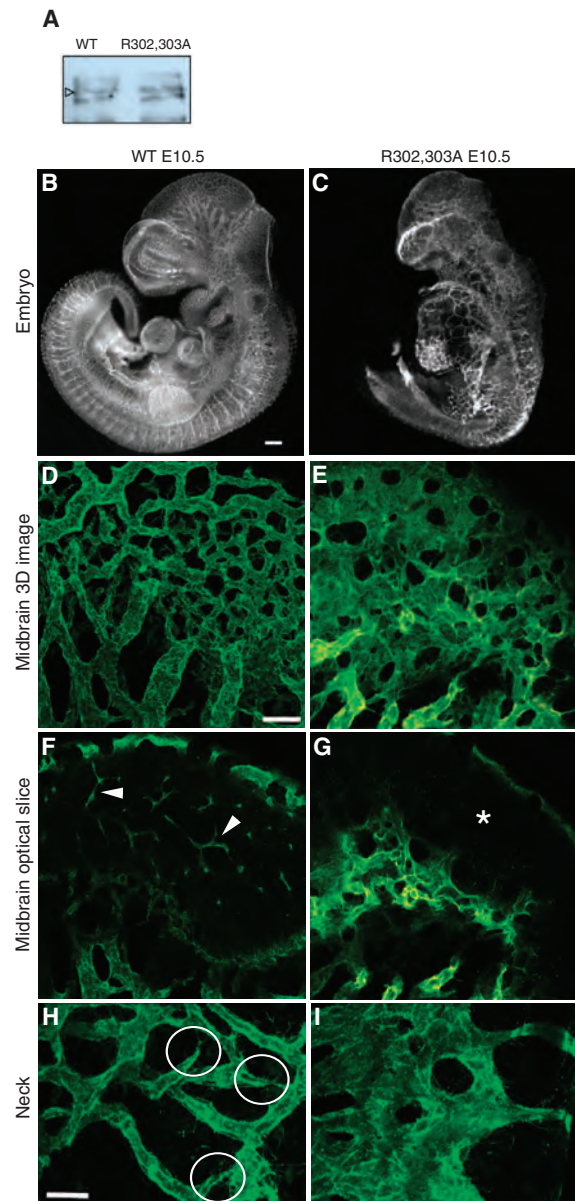

Fig. 6. Incorporating a PH domain mutation into ARAP3, which uncouples it from PI3K, causes defective angiogenesis. (A) ARAP3 protein abundance is not affected by the presence of a point mutation in the most N-terminal PH domains as judged by Western blotting of endothelial cell populations derived from WT and $Arap3^{R302,303A/R302,303A}$ (R302,303A) yolk sacs. (B and C) Representative images of E10.5 WT (B) (n = 24) and $Arap3^{R302,303A/R302,303A}$ (C) (n = 16) embryos whole-mount–stained for endomucin and analyzed with wide-field epifluorescence. Scale bar, 0.25 mm. (D and E) Representative 3D reconstructions of E10.5 endomucin-stained WT (D) (n = 14 embryos) and $Arap3^{R302,303A/R302,303A}$ (E) (n = 13 embryos) midbrains. Scale bar, 90 μm. (F and G) Optical sections through the midbrains shown in (D) and (E). The sinus in the $Arap3^{R302,303A/R302,303A}$ head is marked by an asterisk, and capillaries in the control brain are indicated by arrowheads. (H and I) Representative 3D reconstructions of E10.5 endomucin-stained WT (H) and $Arap3^{R302,303A/R302,303A}$ (I) embryonic necks. Abundant new sprouts are visible in the WT (ovals) but not in the mutant tissue.

However, the embryonic angiogenesis phenotype in PI3Kα D933A knock-in mice does not depend on a change in growth properties, but on a migratory defect of endothelial cells (5), which was regulated by RhoA, making Akt an unlikely signaling intermediate. Accordingly, we observed that inhibiting Akt did not alter sprouting angiogenesis of allantois explants. As in PI3Kα D933A knock-ins, endothelial cell proliferation was not affected in $Arap3^{-/-}$ embryos. Our work points to ARAP3 as a major PI3K effector that regulates angiogenesis.

Our analysis of allantois explants ex vivo, as well as of embryonic hindbrains and necks, demonstrated that ARAP3 (and PI3Kα) is particularly important for the regulation of sprouting angiogenesis. Time-lapse imaging in zebra fish has demonstrated that the formation of new sprouts during angiogenesis is a dynamic process that depends on cell migration (27).

ARAP3's catalytic activities suggest that its effects on angiogenesis may be due to regulation of Arf6 and RhoA, and our analysis of their global catalytic activities in ARAP3-depleted HUVECs supports such a view. Given that PI3K activation causes localized generation of PtdIns(3,4,5)P₃ (28–30) and that the PtdIns(3,4,5)P₃-driven plasma membrane recruitment of the effector ARAP3 is a requirement for its catalytic activity, these global measurements may underestimate any local changes that are attributable to ARAP3. To measure such local changes in the activities of ARAP3's substrates, one would need to use biosensors, such as fluorescence resonance energy transfer (FRET) probes, as has been done in randomly migrating fibroblasts (31, 32).

Both Arf6 and RhoA proteins are well-established regulators of cell motility in other systems (32, 33). Loss of $Arf6$ is embryonically lethal in mice as a result of a defect in hepatic cord formation (34); however, angiogenesis was not investigated in-depth in these mice. However, there is previous evidence for a role of Arf6 in angiogenesis (35, 36). Similarly, although no phenotype for RhoA knockout mice has yet been reported, there is evidence for a role of RhoA in angiogenesis (37). Therefore, future work will be directed to the generation of Arf GAP- and Rho GAP-dead $Arap3$ knock-in mice to assess the contributions of ARAP3's two catalytic activities to its role in the regulation of developmental angiogenesis.

MATERIALS AND METHODS

Generation of Arap3 mouse models
Preparation of targeting vectors, breeding of mouse models, genotyping, and probes used for in situ hybridizations are described in the Supplementary Materials.

Generation of yolk sac–derived endothelial cell populations
Yolk sacs were harvested at E9.5. Cells were dissociated in 0.1% collagenase (Sigma) before being seeded into gelatin-coated tissue culture plates with α Minimum Essential Medium (Gibco) containing 20% fetal calf serum (FCS; Invitrogen), VEGF (5 ng/ml; Autogen Bioclear), and heparin (12 U/ml; Sigma). Cultures were kept in a humidified tissue culture incubator at 37°C and 5% CO_2. Adherent cells were selected by repeated changes of medium during the following day and then allowed to differentiate in culture for 10 days. Endothelial identity of cell populations generated in this way was assessed by immunofluorescence with a rabbit antibody against VEGF receptor 2 (VEGFR2) (Abcam) and a secondary antibody against rabbit conjugated to Alexa Fluor 488 (Molecular Probes). This showed that >90% of the cells were endothelial.

Whole-mount immunofluorescence
Embryos were dissected, rinsed in phosphate-buffered saline (PBS), and fixed overnight in 4% paraformaldehyde, followed by 2 hours of blocking in PBS, 0.2% Triton X-100, and 0.3% nonfat milk powder. Embryos were incubated overnight with suitable antibodies [rat antibody against endomucin (Santa Cruz Biotechnology), rabbit antibody against phosphohistone H3 (Cell Signaling)] in block. Embryos were washed for 3 hours with PBS and 0.2% Triton X-100 before being incubated for 5 hours with a secondary antibody in block [antibody against rat conjugated to Alexa Fluor 488 or antibody against rabbit conjugated to Alexa Fluor 568 (Molecular Probes); sometimes, Hoechst 33342 (Sigma) was added to visualize nuclei]. After 3 hours of washing, embryos were fixed for 1 hour in PBS containing 2% paraformaldehyde and 0.1% glutaraldehyde and then stored in PBS and 50% glycerol. All steps were performed with ice-cold buffers at 4°C. Samples were mounted onto slides with DABCO mounting medium and visualized with an inverted epifluorescence microscope (Cell^R) or a confocal microscope (FV1000; both from Olympus). Three-dimensional (3D) reconstructions and 3D slices were generated with the 3D opacity and 3D slice tools from Volocity software. For analysis of defects in heterozygous animals, an identical developmental stage of wild type and $Arap3^{+/-}$ was ensured by comparing individuals with identical somite numbers (E10.5) or
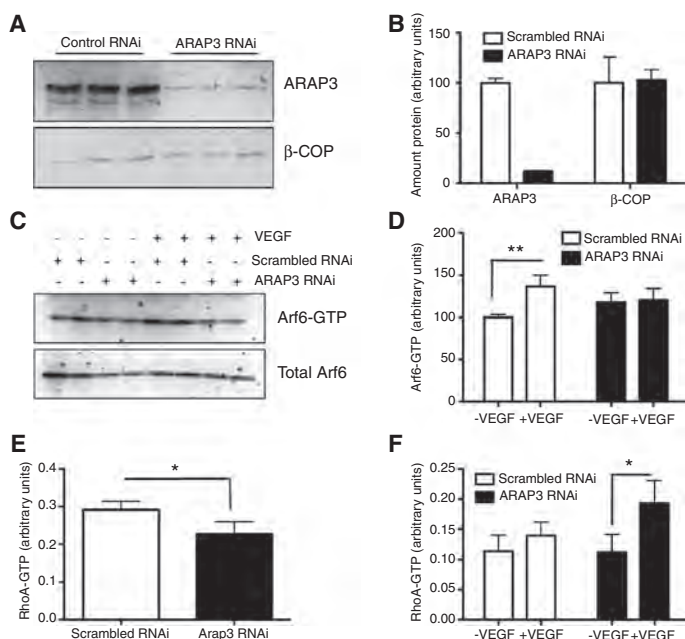

Fig. 7. ARAP3 signals through its effectors Arf6 and RhoA. (**A**) Representative Western blot from ARAP3 or scrambled RNAi-transfected EA926.hy cells. Lanes are from triplicate transfections. The blot was probed with an antiserum for ARAP3 and the loading control β-COP. (**B**) Densitometry of the blot shown in (A). Analysis was performed with the densitometry tool in ImageJ. (**C**) Representative example of an Arf6 pull-down from EA926.hy cells transfected with RNAi directed against ARAP3 or scrambled RNAi, serum-starved, and stimulated with vehicle or VEGF (25 ng/ml) for 5 min. The top panel represents the pulled-down Arf6-GTP; the bottom panel represents 5% of the total lysates for each pull-down reaction. (**D**) Integrated results from four separate Arf6 pull-down assays analyzed by densitometry. (**E** and **F**) Integrated results from four independent G-LISA RhoA activity assays, performed with RNAi-transfected cells growing in the presence of serum (E) or that had been serum-starved and stimulated for 5 min with vehicle or VEGF (25 ng/ml) (F). All bars in the graphs show mean ± SEM. Statistical significance was determined by paired Student's t tests. *$P < 0.05$; **$P < 0.01$.

limb developmental stage (E11.5). All experiments were carried out with at least three different embryos for each genotype analyzed.

Colony assays

Yolk sacs from E9.5 embryos were mechanically disrupted to obtain a single-cell suspension, counted, and resuspended into complete methylcellulose medium containing recombinant stem cell factor (SCF), interleukin-3 (IL-3), IL-6, and erythropoietin (STEMCELL Technologies). Cell suspensions from each yolk sac were split into duplicate plates and left to grow in a humidified atmosphere at 37°C for 3 days. Erythroid cells were detected by staining hemoglobin with 2,7-diaminofluorene (Sigma). Erythrocyte, myeloid, and mixed colonies were counted.

P-Sp explants

E8.5 P-Sp explants were performed as described previously (12). After 14 days in culture, explants were fixed in 4% paraformaldehyde. Endogenous peroxidases were inactivated with PBS and 4% H_2O_2 for 1 hour at room temperature in the dark. Explants were then washed with PBS, blocked for 2 hours in PBS, 0.2% Triton X-100, and 0.3% nonfat milk powder, and incubated overnight with rat antibody against endomucin (Santa Cruz Biotechnology) and rat antibody against CD31 (BD Biosciences) in block. Explants were washed for 5 hours with PBS and 0.2% Triton X-100 before being incubated overnight with a horseradish peroxidase–conjugated antibody against rat (Abcam) in blocking buffer. All steps were performed with ice-cold buffers at 4°C. After 3 hours of washing, signal was revealed with diaminobenzidine (DAB; Sigma). Explants were rinsed in PBS and imaged with a Zeiss Axiophot light microscope.

Allantois explants

Allantoises were dissected from E8.5 embryos and cultured for 18 hours in eight-well μ-Slides (Ibidi) coated with bovine fibronectin (Sigma) in Dulbecco's modified Eagle's medium (DMEM; Gibco) supplemented with 10% FCS (Invitrogen) in a humidified incubator at 37°C and 5% CO_2. When inhibitors were used, they were made up in dimethyl sulfoxide (DMSO) and added into the growth medium at the beginning of the culture; in such experiments, wild-type controls received DMSO. Inhibitors were obtained from Calbiochem and used at the following concentrations: TGX-221, 40 nM; PI-103, 0.25 μM; and AktI, 0.3 μM. Whole-mount immunofluorescence was carried out as described for embryos and yolk sacs except that a rat antibody against vascular endothelial cadherin (VE-cadherin; BD Biosciences) was used together with antibody against endomucin. Pictures of the explants were taken with an inverted epifluorescence microscope (Olympus Cell[R]).

Analysis of allantois explants

Allantois explants were analyzed with ImageJ (http://rsbweb.nih.gov/ij/). Vessel segmentation was performed after application of Hessian-based multiscale filter (38). Binary images were then skeletonized (39) and junctions were detected as pixels with more than two neighbors. The area of the explants was calculated as the area of the convex hull polygon containing the explant. The number of junctions per area of explant was used as an assessment of vasculature complexity. Statistical analysis was performed with GraphPad Prism 5 for graphs in Fig. 3 and fig. S12 with Student's t test, and with PASW 18 for Fig. 5 with a univariate analysis of variance (Games-Howell post hoc test).

Angiogenesis in the hindbrain

Hindbrains were dissected from surrounding tissue and then fixed, dehydrated, and rehydrated as previously described (15) before being wholemount–stained for endomucin as described above. All samples were analyzed from the ventricular side. To count branches, we took photographs of several areas (0.4 mm²) per hindbrain using an epifluorescence Cell[R] microscope (Olympus); for demonstration purposes (Fig. 4), representative images were also taken with a confocal microscope (FV1000, Olympus).

Knockdown of ARAP3

EA926.hy cells were cultured as described (24) and reverse-transfected with ON-TARGETplus SMARTpool RNAi oligos directed against human ARAP3 (GUAAUGAGAUAGUACAGUU, GCAGAAAUGUGCGGCU-CUA, ACACGGGAGUGGACAGUGA, GAACGGGAGUGGC-CUUUGG) or as a control with the ON-TARGETplus nontargeting RNAi pool (Dharmacon) with DharmaFECT 4 (Dharmacon) according to the manufacturer's instructions. Cells were used for experiments 60 hours after transfection.

Activity assays for small GTPases

Assays were carried out with RNAi-transfected growing, serum-starved, or VEGF (Autogen Bioclear)–stimulated cells in 6-cm dishes. Arf6-GTP was measured with a "pull-down" assay using glutathione S-transferase (GST)–GgA coupled to glutathione Sepharose beads as a bait, as previously described (40). Fractions of the clarified lysate and washed beads were subjected to SDS–polyacrylamide gel electrophoresis (SDS-PAGE), transferred onto a polyvinylidene difluoride membrane, and immunoblotted with an antibody specific for Arf6 (Santa Cruz Biotechnology). RhoA-GTP was measured according to the manufacturer's instruction with an absorbance-based G-LISA assay (Cytoskeleton).

SUPPLEMENTARY MATERIALS

www.sciencesignaling.org/cgi/content/full/3/145/ra76/DC1
Materials and Methods
Fig. S1. Generation of a conditional *Arap3* knockout mouse.
Fig. S2. Loss of ARAP3 in the germ line, in embryonic tissues, or in the endothelial compartment, or incorporation of a PH domain point mutation causes defects in the embryo and yolk sac.
Fig. S3. Analysis of blood flow in *Arap3*⁻/⁻ embryos.
Fig. S4. Analysis of the placental phenotype in *Arap3* mutants.
Fig. S5. *Arap3*⁻/⁻ embryos die due to an endothelial cell–autonomous vascular defect.
Fig. S6. Vascular remodeling, but not hematopoiesis, is affected in *Arap3*⁻/⁻ yolk sacs.
Fig. S7. *Arap3*⁺/⁻ embryos show a mild, transient delay in angiogenesis.
Fig. S8. The *Arap3*⁻/⁻ angiogenesis defect is not due to enhanced endothelial cell proliferation.
Fig. S9. Appearance of the allantois before explant culture.
Fig. S10. Analysis of sprouting angiogenesis.
Fig. S11. Generation of the *Arap3*^R302,303A/R302,303A^ PH domain knock-in mouse.
Fig. S12. A PH domain point mutation in ARAP3, which uncouples it from PI3K, causes defective angiogenesis.
Fig. S13. ARAP3 knockdown in HUVECs.
Table S1. Genotypes of litters from *Arap3*⁺/⁻ intercrosses.
Table S2. Genotypes of litters from *Arap3*⁺/R302,303A intercrosses.
References

REFERENCES AND NOTES

1. W. Risau, Mechanisms of angiogenesis. *Nature* **386**, 671–674 (1997).
2. R. H. Adams, K. Alitalo, Molecular regulation of angiogenesis and lymphangiogenesis. *Nat. Rev. Mol. Cell Biol.* **8**, 464–478 (2007).
3. P. T. Hawkins, K. E. Anderson, K. Davidson, L. R. Stephens, Signalling through Class I PI3Ks in mammalian cells. *Biochem. Soc. Trans.* **34**, 647–662 (2006).
4. T. L. Yuan, H. S. Choi, A. Matsui, C. Benes, E. Lifshits, J. Luo, J. V. Frangioni, L. C. Cantley, Class 1A PI3K regulates vessel integrity during development and tumorigenesis. *Proc. Natl. Acad. Sci. U.S.A.* **105**, 9739–9744 (2008).
5. M. Graupera, J. Guillermet-Guibert, L. C. Foukas, L. K. Phng, R. J. Cain, A. Salpekar, W. Pearce, S. Meek, J. Millan, P. R. Cutillas, A. J. Smith, A. J. Ridley, C. Ruhrberg, H. Gerhardt, B. Vanhaesebroeck, Angiogenesis selectively requires the p110α isoform of PI3K to control endothelial cell migration. *Nature* **453**, 662–666 (2008).
6. S. Krugmann, K. E. Anderson, S. H. Ridley, N. Risso, A. McGregor, J. Coadwell, K. Davidson, A. Eguinoa, C. D. Ellson, P. Lipp, M. Manifava, N. Ktistakis, G. Painter,

J. W. Thuring, M. A. Cooper, Z. Y. Lim, A. B. Holmes, S. K. Dove, R. H. Michell, A. Grewal, A. Nazarian, H. Erdjument-Bromage, P. Tempst, L. R. Stephens, P. T. Hawkins, Identification of ARAP3, a novel PI3K effector regulating both Arf and Rho GTPases, by selective capture on phosphoinositide affinity matrices. *Mol. Cell* 9, 95–108 (2002).

7. S. Krugmann, R. Williams, L. Stephens, P. T. Hawkins, ARAP3 is a PI3K- and Rap-regulated GAP for RhoA. *Curr. Biol.* 14, 1380–1384 (2004).

8. H. E. Craig, J. Coadwell, H. Guillou, S. Vermeren, ARAP3 binding to phosphatidylinositol-(3,4,5)-trisphosphate depends on N-terminal tandem PH domains and adjacent sequences. *Cell. Signal.* 22, 257–264 (2010).

9. F. Schwenk, U. Baron, K. Rajewsky, A *cre*-transgenic mouse strain for the ubiquitous deletion of *loxP*-flanked gene segments including deletion in germ cells. *Nucleic Acids Res.* 23, 5080–5081 (1995).

10. S. Hayashi, P. Lewis, L. Pevny, A. P. McMahon, Efficient gene modulation in mouse epiblast using a *Sox2Cre* transgenic mouse strain. *Mech. Dev.* 119 (Suppl. 1), S97–S101 (2002).

11. Y. Y. Kisanuki, R. E. Hammer, J. Miyazaki, S. C. Williams, J. A. Richardson, M. Yanagisawa, Tie2-Cre transgenic mice: A new model for endothelial cell-lineage analysis in vivo. *Dev. Biol.* 230, 230–242 (2001).

12. K. Kumano, S. Chiba, A. Kunisato, M. Sata, T. Saito, E. Nakagami-Yamaguchi, T. Yamaguchi, S. Masuda, K. Shimizu, T. Takahashi, S. Ogawa, Y. Hamada, H. Hirai, Notch1 but not Notch2 is essential for generating hematopoietic stem cells from endothelial cells. *Immunity* 18, 699–711 (2003).

13. E. D. Perryn, A. Czirok, C. D. Little, Vascular sprout formation entails tissue deformations and VE-cadherin-dependent cell-autonomous motility. *Dev. Biol.* 313, 545–555 (2008).

14. K. M. Downs, R. Temkin, S. Gifford, J. McHugh, Study of the murine allantois by allantoic explants. *Dev. Biol.* 233, 347–364 (2001).

15. C. Ruhrberg, H. Gerhardt, M. Golding, R. Watson, S. Ioannidou, H. Fujisawa, C. Betsholtz, D. T. Shima, Spatially restricted patterning cues provided by heparin-binding VEGF-A control blood vessel branching morphogenesis. *Genes Dev.* 16, 2684–2698 (2002).

16. A. Uemura, S. Kusuhara, H. Katsuta, S. Nishikawa, Angiogenesis in the mouse retina: A model system for experimental manipulation. *Exp. Cell Res.* 312, 676–683 (2006).

17. Z. A. Knight, B. Gonzalez, M. E. Feldman, E. R. Zunder, D. D. Goldenberg, O. Williams, R. Loewith, D. Stokoe, A. Balla, B. Toth, T. Balla, W. A. Weiss, R. L. Williams, K. M. Shokat, A pharmacological map of the PI3-K family defines a role for p110α in insulin signaling. *Cell* 125, 733–747 (2006).

18. S. P. Jackson, S. M. Schoenwaelder, I. Goncalves, W. S. Nesbitt, C. L. Yap, C. E. Wright, V. Kenche, K. E. Anderson, S. M. Dopheide, Y. Yuan, S. A. Sturgeon, H. Prabaharan, P. E. Thompson, G. D. Smith, P. R. Shepherd, N. Daniele, S. Kulkarni, B. Abbott, D. Saylik, C. Jones, L. Lu, S. Giuliano, S. C. Hughan, J. A. Angus, A. D. Robertson, H. H. Salem, PI 3-kinase p110β: A new target for antithrombotic therapy. *Nat. Med.* 11, 507–514 (2005).

19. J. Chen, P. R. Somanath, O. Razorenova, W. S. Chen, N. Hay, P. Bornstein, T. V. Byzova, Akt1 regulates pathological angiogenesis, vascular maturation and permeability in vivo. *Nat. Med.* 11, 1188–1196 (2005).

20. T. L. Phung, K. Ziv, D. Dabydeen, G. Eyiah-Mensah, M. Riveros, C. Perruzzi, J. Sun, R. A. Monahan-Earley, I. Shiojima, J. A. Nagy, M. I. Lin, K. Walsh, A. M. Dvorak, D. M. Briscoe, M. Neeman, W. C. Sessa, H. F. Dvorak, L. E. Benjamin, Pathological angiogenesis is induced by sustained Akt signaling and inhibited by rapamycin. *Cancer Cell* 10, 159–170 (2006).

21. Z. Z. Yang, O. Tschopp, M. Hemmings-Mieszczak, J. Feng, D. Brodbeck, E. Perentes, B. A. Hemmings, Protein kinase Bα/Akt1 regulates placental development and fetal growth. *J. Biol. Chem.* 278, 32124–32131 (2003).

22. B. Dummler, O. Tschopp, D. Hynx, Z. Z. Yang, S. Dirnhofer, B. A. Hemmings, Life with a single isoform of Akt: Mice lacking Akt2 and Akt3 are viable but display impaired glucose homeostasis and growth deficiencies. *Mol. Cell. Biol.* 26, 8042–8051 (2006).

23. J. Bain, L. Plater, M. Elliott, N. Shpiro, C. J. Hastie, H. McLauchlan, I. Klevernic, J. S. Arthur, D. R. Alessi, P. Cohen, The selectivity of protein kinase inhibitors: A further update. *Biochem. J.* 408, 297–315 (2007).

24. C. J. Edgell, C. C. McDonald, J. B. Graham, Permanent cell line expressing human factor VIII-related antigen established by hybridization. *Proc. Natl. Acad. Sci. U.S.A.* 80, 3734–3737 (1983).

25. B. A. Bryan, E. Dennstedt, D. C. Mitchell, T. E. Walshe, K. Noma, R. Loureiro, M. Saint-Geniez, J. P. Campaigniac, J. K. Liao, P. A. D'Amore, RhoA/ROCK signaling is essential for multiple aspects of VEGF-mediated angiogenesis. *FASEB J.* 24, 3186–3195 (2010).

26. L. C. Foukas, M. Claret, W. Pearce, K. Okkenhaug, S. Meek, E. Peskett, S. Sancho, A. J. Smith, D. J. Withers, B. Vanhaesebroeck, Critical role for the p110α phosphoinositide-3-OH kinase in growth and metabolic regulation. *Nature* 441, 366–370 (2006).

27. A. F. Siekmann, N. D. Lawson, Notch signalling limits angiogenic cell behaviour in developing zebrafish arteries. *Nature* 445, 781–784 (2007).

28. P. S. Costello, M. Gallagher, D. A. Cantrell, Sustained and dynamic inositol lipid metabolism inside and outside the immunological synapse. *Nat. Immunol.* 3, 1082–1089 (2002).

29. M. Nishio, K. Watanabe, J. Sasaki, C. Taya, S. Takasuga, R. Iizuka, T. Balla, M. Yamazaki, H. Watanabe, R. Itoh, S. Kuroda, Y. Horie, I. Forster, T. W. Mak, H. Yonekawa, J. M. Penninger, Y. Kanaho, A. Suzuki, T. Sasaki, Control of cell polarity and motility by the PtdIns(3,4,5)P3 phosphatase SHIP1. *Nat. Cell Biol.* 9, 36–44 (2007).

30. G. Halet, P. Viard, J. Carroll, Constitutive PtdIns(3,4,5)P3 synthesis promotes the development and survival of early mammalian embryos. *Development* 135, 425–429 (2008).

31. O. Pertz, L. Hodgson, R. L. Klemke, K. M. Hahn, Spatiotemporal dynamics of RhoA activity in migrating cells. *Nature* 440, 1069–1072 (2006).

32. M. Machacek, L. Hodgson, C. Welch, H. Elliott, O. Pertz, P. Nalbant, A. Abell, G. L. Johnson, K. M. Hahn, G. Danuser, Coordination of Rho GTPase activities during cell protrusion. *Nature* 461, 99–103 (2009).

33. L. C. Santy, K. S. Ravichandran, J. E. Casanova, The DOCK180/Elmo complex couples ARNO-mediated Arf6 activation to the downstream activation of Rac1. *Curr. Biol.* 15, 1749–1754 (2005).

34. T. Suzuki, Y. Kanai, T. Hara, J. Sasaki, T. Sasaki, M. Kohara, T. Maehama, C. Taya, H. Shitara, H. Yonekawa, M. A. Frohman, T. Yokozeki, Y. Kanaho, Crucial role of the small GTPase ARF6 in hepatic cord formation during liver development. *Mol. Cell. Biol.* 26, 6149–6156 (2006).

35. S. Ikeda, M. Ushio-Fukai, L. Zuo, T. Tojo, S. Dikalov, N. A. Patrushev, R. W. Alexander, Novel role of ARF6 in vascular endothelial growth factor-induced signaling and angiogenesis. *Circ. Res.* 96, 467–475 (2005).

36. C. A. Jones, N. Nishiya, N. R. London, W. Zhu, L. K. Sorensen, A. C. Chan, C. J. Lim, H. Chen, Q. Zhang, P. G. Schultz, A. M. Hayallah, K. R. Thomas, M. Famulok, K. Zhang, M. H. Ginsberg, D. Y. Li, Slit2-Robo4 signalling promotes vascular stability by blocking Arf6 activity. *Nat. Cell Biol.* 11, 1325–1331 (2009).

37. G. P. van Nieuw Amerongen, V. W. van Hinsbergh, Role of ROCK I/II in vascular branching. *Am. J. Physiol. Heart Circ. Physiol.* 296, H903–H905 (2009).

38. A. F. Frangi, W. J. Niessen, K. L. Vincken, M. A. Vergever, in *MICCAI 98*, W. M. Wells, A. Colchester, S. Delp, Eds. (Springer Verlag, Berlin, 1998), vol. 1496, pp. 130–137.

39. T. C. Lee, R. L. Kashyap, C. N. Chu, Building skeleton models via 3-D medial surface axis thinning algorithms. *CVGIP: Graph. Models Image Process.* 56, 462–478 (1994).

40. L. C. Santy, J. E. Casanova, Activation of ARF6 by ARNO stimulates epithelial cell migration through downstream activation of both Rac1 and phospholipase D. *J. Cell Biol.* 154, 599–610 (2001).

The following resources related to this article are available online at http://stke.sciencemag.org.
This information is current as of July 7, 2015.

Article Tools	Visit the online version of this article to access the personalization and article tools: http://stke.sciencemag.org/content/3/145/ra76
Supplemental Materials	*"Supplementary Materials"* http://stke.sciencemag.org/content/suppl/2010/10/22/3.145.ra76.DC1.html
Related Content	The editors suggest related resources on *Science*'s sites: http://stke.sciencemag.org/content/sigtrans/3/116/ra26.full.html http://stke.sciencemag.org/content/sigtrans/3/145/pc19.full.html http://stke.sciencemag.org/content http://stke.sciencemag.org/content/sigtrans/6/271/pc10.full.html http://stke.sciencemag.org/content http://stke.sciencemag.org/content/sigtrans/7/347/ra97.full.html
References	This article cites 39 articles, 13 of which you can access for free at: http://stke.sciencemag.org/content/3/145/ra76#BIBL
Glossary	Look up definitions for abbreviations and terms found in this article: http://stke.sciencemag.org/cgi/glossarylookup
Permissions	Obtain information about reproducing this article: http://www.sciencemag.org/about/permissions.dtl